STABILITY EVALUATION OF ROTOR/BEARING SYSTEM

BY PERTURBATION TESTS

Donald E. Bently and Agnieszka Muszynska
Bently Nevada Corp.
P.O. Box 157
Minden, Nevada 89423

SUMMARY

The paper presents the stability study of rotor/bearing systems. Even though it was limited to study of a fully lubricated bearing subject to oil whirl, and further limited to low eccentricity region for linearity and with only one type of lubricant, it can be seen that the perturbation methodology, together with the sorting of the impedance terms into direct and quadrature with respect to input force can be very useful to the general study of stability. Further, the concept of active feedback should assist to increase knowledge in rotor system stability. While there remains a large amount of study to be accomplished, perhaps some more tools are available to assist this field of analysis.

INTRODUCTION

The problem of rotor vibration in plain fluid bearing becomes more and more serious as operating speeds of turbomachinery continually increase. Two of the most significant sources of vibrations are fluid lubricated bearings and seals. Despite the high interest of field engineers and researchers which has followed the widespread application of oil/gas bearings and seals, the problems created by their hydrodynamic actions in turbomachines are still not solved completely [1-18].

This paper shows that the dynamic behavior of a rotor and its stability can be modeled as an active feedback mechanism, which should greatly help in clarifying the stability problems of rotor system. It further shows testing and data techniques for bearings and seals, and the evaluation of the performance of a perturbation test bearing.

The principal observed dynamic phenomena due to the lubricant action during shaft rotation are known as oil whirl and oil whip. Oil whirl appears at rotational speeds lower than twice the first bending critical speed of the rotor (corresponding to its first natural frequency), as a forward circular motion of the journal with the frequency nearly equal to half the speed of rotation. This motion is related to a loss of stability of a pure rotational motion (about a central position of the journal in the bearing, or more generally - an equilibrium position, determined by the static load) and creation of a stable steady circular motion with an amplitude affected by nonlinear factors of the oil film. In the performance of real machines, oil whirl may cause serious machine damage since the level of the steady-state whirling amplitude may exceed admitted tolerances of vibration.

Oil whip also has the character of forward motion, but unlike oil whirl, is locked to the frequency of the first self balance resonance (critical speed) of the rotor. The rotational speed must be of at least twice the resonance speed for oil whip instability to occur. Sometimes the rotor goes unstable in oil whirl, then converts

to oil whip when higher rotative speeds are reached. Oil whirl is not known to occur at higher speeds than oil whip.

In earlier years it was believed that for all of the forward circular instabilities that the range of rotative speeds from 2 to 2.5 times the self-balance resonance speed was required. However, more recent works [1] show that such instabilities may occur at any rotative speed ratio with respect to balance resonances, depending on the type of instability. Some machines in the field with severe gas whip problems show that this instability cannot be cured with the machine rotational speed below the first self balance resonance.

The literature on oil whirl/whip phenomena is quite rich [1-18]. The results concerning the loss of stability of the pure rotational rotor motion are usually presented in the form of stability charts describing the behavior of the rotor in the vicinity of the steady equilibrium position for different variable parameters. The stability rules indicated by different authors rarely agree in detail. This is not surprising - rotor response is very sensitive to slight variations in parameters (e.g., a change of temperature by a few degrees, or minor geometric asymmetry in the bearing may stabilize the rotor), and it has not been recognized that the active feedback is involved.

Classical analysis of the rotor/bearing systems usually starts from the very general Euler-Navier-Stokes equations. The solution of these equations, which may supply information concerning magnitude and functional relationship of hydrodynamic forces is unfortunately not easy to obtain. Analytical solutions require a lot of simplfying assumptions (such as idealized boundary conditions, neglecting thermal effects, ideal characteristics of lubricant, assumed pattern of the pressure distribution, neglecting curvature and capillarity effects of the lubricant, laminar flow, etc.). The resulting solution represents, then, only a rough approximation, as some of the neglected factors may happen to be dominant.

Numerical solutions of the Euler-Navier-Stokes equations, requiring, just as much, a number of simplifying assumptions, involve a lot of time-consuming computations [6] and can solve only some particular problems. Progress in computer facilities and numerical techniques, however, improves the possibility of achieving solutions, which allow for rotor/bearing coupling of motion and further parametric analysis. Parallel to the progress in computer sciences, a remarkable progress in experimental techniques and measurement facilities has been observed. The experimental results bring better understanding of dominating phenomena occurring during rotor/bearing motion. This, in turn, will clarify eventually the simplifying assumptions introduced in theoretical analyses.

In the present paper an experimental method of identifying the hydrodynamic forces in a plain cylindrical bearing during the oil whirl condition will be dicussed. The results are applicable to rotor/bearing or rotor/seal systems. The approach, based on analysis of forced response of the perturbed system, presents a continuation of previous research [7,8,9,12,13]. The mathematical model of the system considered is based on the linear theory of the rotor motion and fluid flow effects, as this series of tests have been deliberately run at low eccentricity numbers (generally less than 0.5).

The agreement of the experimental results and the predicted motion is very good. The method of investigation is shown to be very effective and sensitive to any parametric variation, so that it can be highly recommended in many applications.

TEST ROTOR SYSTEM AND THE PHYSICAL MODEL

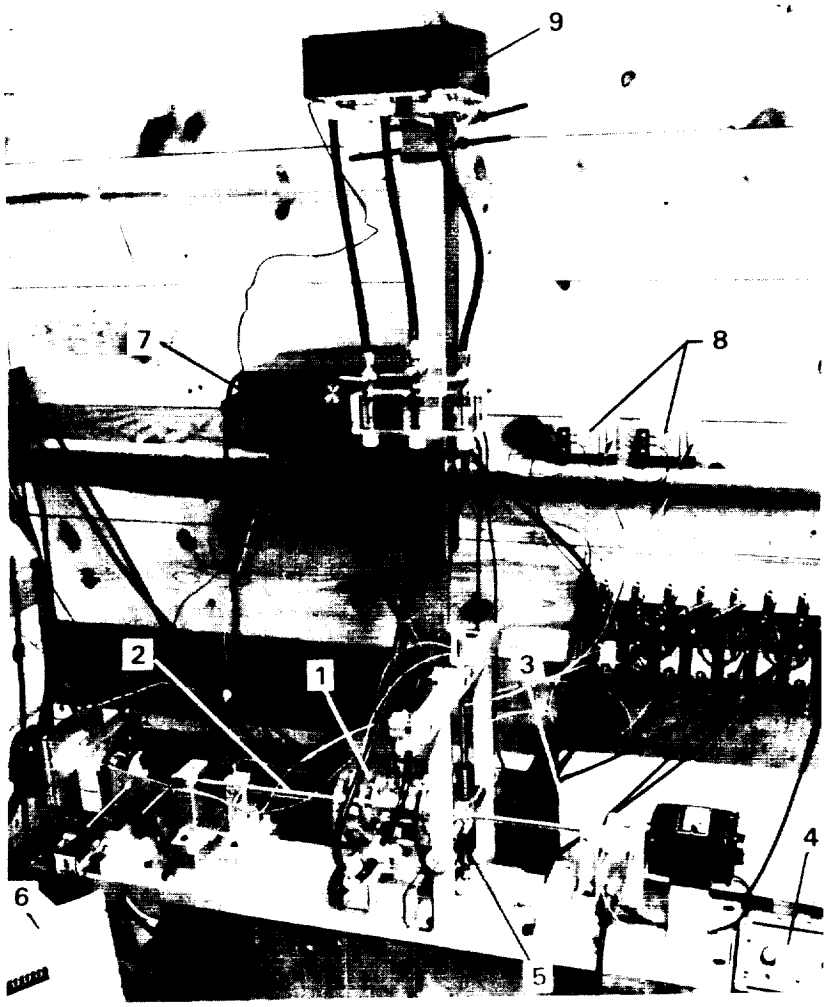

Figure 1. - Rotor test rig. 1 - Bearing, 2 - Main shaft, 3 - Perturbing shaft, 4 - Perturbing speed controller, 5 - Additional springs, 6 - Main shaft tachometer, 7 - Thermometer, 8 - Proximitors, 9 - Perturbed Reservoir.

The experimental rig to perform the perturbation test consists of two shafts with circular cross sections (Figs. 1,2). The main shaft rotates at the constant speed ω_R (being quite well below the first critical speed) in a rolling, pivoting bearing and in a plain cylindrical oil bearing with diameter D=2" axial length L=1.5" and radial clearance C=0.015". The second shaft rotating at perturbing speed ω_p in a pivoting bearing and a rolling antifriction bearing, is attached to the journal of the main shaft at the oil bearing. The transparent bearing, fed by blue dyed oil type ISO-VG-32 from an outboard tank with a constant pressure p=7100 N/m^2 permits direct observation of the distribution of the lubricant within the bearing .

Both shafts are driven by separate electric motors (0.75 HP for the main rotor, 0.1 HP for the perturbing one) through a flexible rubber coupling. For compensating weight of two shafts, a pulling vertical force is introduced in such a manner that during rotation of the main shaft, its response is a pure rotating motion in the center of the bearing. For this purpose, the main shaft is also straightened and balanced. At the same section of the shaft the additional symmetric springs can be introduced. The perturbing force is created by a controlled unbalance at the second shaft (calibrated unbalance masses attached to a single light disk mounted on the shaft). The unbalance inertia force is then proportional to the square of the perturbing speed ω_p .

The motion of the shaft journal is observed by two displacement motion, noncontacting probes (vertically and horizontally located) plus a Keyphasor probe to provide accurate phase and speed signals. Additionally the constant rotational speed of the main shaft and slowly variable rotation speed of the perturbing shaft are recorded. A special device designed to control constant angular acceleration of the perturbing shaft was used. The Keyphasor, horizontal and vertical probe signals, filtered to

the main (perturbing) frequency, were continuously observed on the oscilloscope monitor (orbits and time variable displays) and stored in the computer. The computer then provides numerical results and graphical representation of the amplitude/phase/frequency relationships, or their derivatives ("Direct" and "Quadrature" Impedances, see expressions (9) and (10)). The physical model of the system is presented in Fig 2.

MATHEMATICAL MODEL OF THE SYSTEM

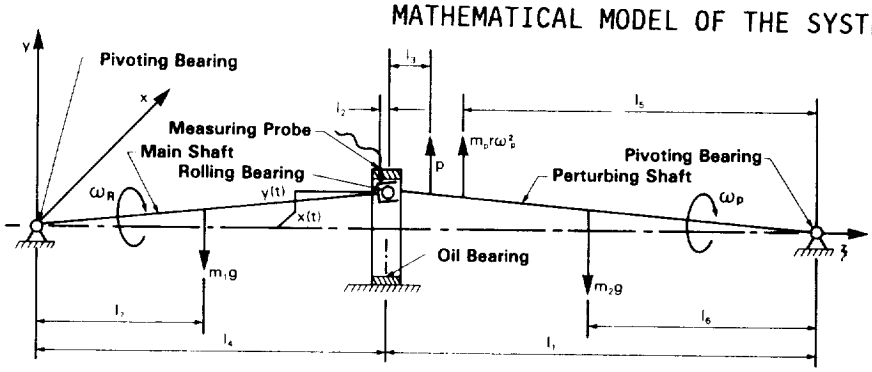

Figure 2. - Physical model of system.

The mathematical model is based on the assumption of "small" deflections, allowing for linerization. The angular motions of the shafts are then approximated by their linear radial deflections. The hydrodynamic forces are introduced in the oil bearing are introduced in their linear approximation. It was assumed that the system has only two degrees of freedom (horizontal (x) and vertical (y) deflections of the main shaft, as seen by the probes). The shafts are supposed rigid. External damping is neglected. With these assumptions, the equation of motion of the system is as follows:

$$M\ddot{z} + (J_1\omega_R + J_2\omega_p)i\dot{z} + Kz + F = U\,\omega_p^2\, e^{i\omega_p t} + i\,P_1\,, \qquad (1)$$

where:

$$M = I_1/\ell_4^2 + I_2/\ell_1^2, \qquad J_1 = I_{1z}/\ell_4^2,$$
$$J_2 = I_{2z}/\ell_1^2, \qquad U = (\ell_4-\ell_2)\ell_5\, m_p\, r/\ell_1\ell_4, \qquad (2)$$
$$P_1 = (\ell_4-\ell_2)[P(\ell_1-\ell_3) - g\,(\ell_1 m_1 \ell_7/\ell_4 + m_2\ell_6)]/\ell_1\ell_4$$

and

$$z = x + iy, \qquad i = \sqrt{-1} \qquad (3)$$

combines in a complex variable the horizontal (x) and vertical (y) deflections of the journal; I_1, I_2, I_{1z}, I_{2z} are moments of inertia of the main (1) and perturbing (2) shafts (about the x or y and z axis), $\ell_1,\ldots,\ell_7$, are corresponding lengths (Fig. 2); ω_R is main shaft rotational speed, ω_p - perturbing shaft rotation speed, K - stiffness coefficient of the additional springs; m_p, r-mass and radius of the controlled unbalance, P - vertical constant pulling force, m_1, m_2 - masses of the main and perturbing rotors, g- gravity acceleration. F represents the hydrodynamic force in the bearing:

$$F = (m + m_t i)\ddot{z} + (d_r - d_t i)\dot{z} + (k_r - \omega_R k_t i)z\,, \qquad (4)$$

where m, m_t, d_r, d_t, k_r and k_t are bearing coefficients.

The full symmetric linear two degree of freedom model of hydrodynamic forces is taken into consideration.

SOLUTION OF THE MATHEMATICAL MODEL

We simplify the mathematical model (1)+(4) neglecting gyroscopic terms (J_2=J_2=0) and the coupling "fluid inertia" term (m_t=0).

If the condition of stability is satisfied,

$$-|f_2| < \omega_R k_t / d_r < |f_1| , \tag{5}$$

where f_1, f_2 are natural frequencies of the free vibration (see Appendix for details), then the dominating solution of (1) will be the forced response:

$$z = A\, e^{i(\omega_p t + \gamma)} + B , \tag{6}$$

where amplitude A and phase angle γ are

$$A = U \omega_p^2 / (D^2 + Q^2)^{1/2} , \tag{7}$$

$$\gamma = \arctan (-Q/D) , \tag{8}$$

with

$$\text{Direct Impedance: } D = -(M + m)\, \omega_p^2 + d_t \omega_p + k_r + K \tag{9}$$

and

$$\text{Quadrature Impedance: } Q = d_r \omega_p - k_t \omega_R . \tag{10}$$

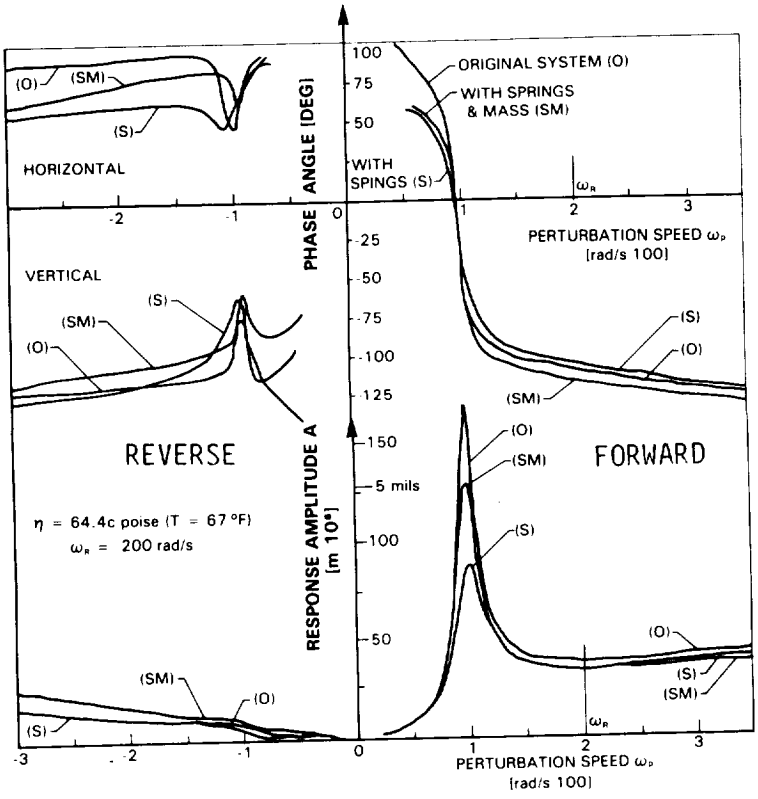

Figure 3. - Phase frequency and amplitude/frequency responses of system.

Note that the phase angle γ corresponds to the attitude angle of the bearing.

The static displacement in the solution (6) is

$$B = \frac{P_1 \left(i(k_r + K) - \omega_R k_t \right)}{(K + k_r)^2 + k_t^2 \omega_R^2} . \tag{11}$$

It will serve for evaluation of the stiffness coefficients by a preload test with no perturbation ($\omega_p = 0$). During the perturbation test (variable ω_p) the preload was eliminated ($P_1 = 0$).

TEST RESULTS. IDENTIFICATION OF THE IMPEDANCES AS FUNCTIONS OF ROTATIONAL SPEED. STABILITY CHECK

The experimental tests produced a set of results for the response amplitude A and phase angle γ versus (slowly varying) perturbation speed. The parameters of the set were rotational speed and temperature. The tests were performed for three cases: with additional springs (System "S"), with additional springs and mass (System "SM") and without

them (original system "0"). Fig. 3 presents an example of the test results for a rotational speed ω_R =200 rad/s. For a perturbation speed slightly less than half of the rotational speed, a well pronounced resonance was observed. This pattern repeated for all values of the rotational speed. In the resonance vicinity, the phase angle sharply changes values between zero and -90°. This behavior corresponds well to the predicted model of the system (see expressions (7), (8)).

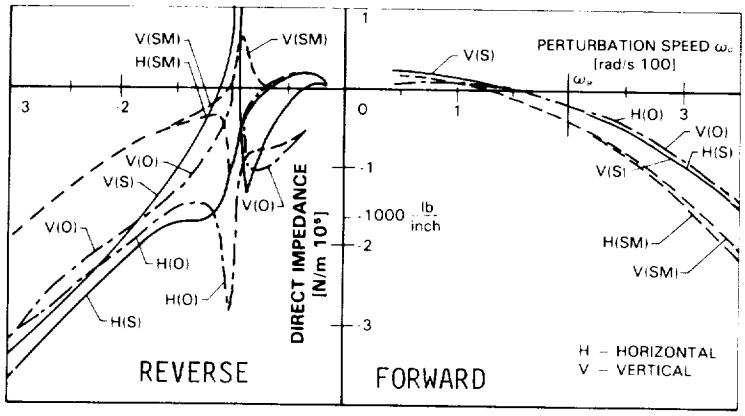

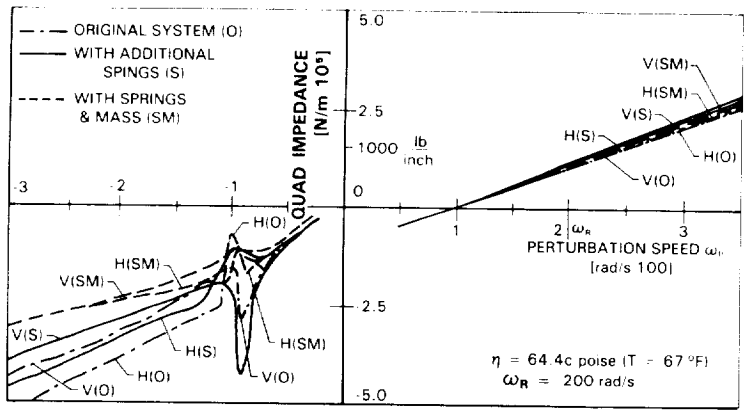

Figure 4. - Impedances versus perturbation speed for three cases.

The system without additional springs and mass shows the highest resonance amplitude. An addition of springs lowers the amplitude considerably.

For the reverse perturbation speed resonance has not been observed although the system attempts to whirl forward. The amplitudes of vibration slowly increase with negative frequency, the phase angle slightly changes at the frequency corresponding to minus half ω_R. Major differences in horizontal and vertical phase angles are due to the 90° difference in probe readings. We observe however, some nonsymmetricity in the system, especially in the $-1/2\omega_R$ frequency region.

The experimental data stored in the computer were transformed into the Direct and Quadrature Impedances:

$$D = U\,\omega_p^2\,\cos\gamma\,/A\,, \qquad Q = -U\,\omega_p^2\,\sin\gamma\,/A \tag{12}$$

An example of the computer generated relationship between Impedances and perturbation speed for ω_R = 200 rad/s is given in Fig. 4. The graphs correspond to the results presented in Fig. 3. In all three cases the symmetry of the system for the forward perturbation speed was maintained - the amplitudes and phases showed to be the same for vertical and horizontal responses, the orbits were circular. At the reverse perturbation speed, we observed differences in horizontal and vertical Impedances.

Figure 5 presents a set of results of the response of the original system "0" for variable rotational speed. All other parameters of the system were kept constant during this test. The Direct Impedances have a roughly parabolic shape, while the Quadrature Impedances are nearly straight lines.

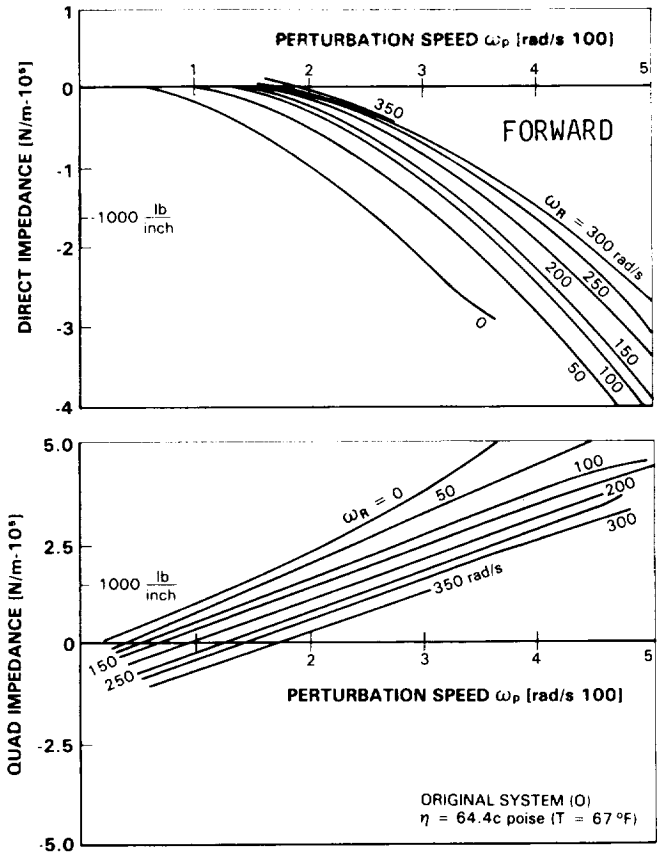

Figure 5. - Impedances versus perturbation speed for variable rotational speed.

The data taken from Fig. 5 served to obtain the cross relation for the Direct Impedance versus rotational speed with the perturbation speed as a parameter (Fig. 6). An analytical approximation to the Direct Impedance as straight line function of the rotational speed has been adapted:

$$D = C_1\omega_R - C_2.$$

The next step of identification was an evaluation of the coefficients C_1 and C_2 as functions of the perturbation speed ω_p. For this purpose, the values of the Direct Impedance at zero perturbation speed and the slopes of the straight lines present in Fig. 6 were crossplotted as functions of the perturbation speed.

For both of these curves the parabolic approximation has been adapted [15]:

$$C_1 = -1.8\cdot10^{-3}\,\omega_p^2 - 2.5\,\omega_p - 200 \text{ [kg/s]}$$

$$C_2 = +0.25\,\omega_p^2 - 950\,\omega_p - 9.5\cdot10^4 \text{ [N/m]}$$

Finally the Direct Impedance is described by for the following analytical form:

$$D/0.77 = -(1.8\cdot10^{-3}\,\omega_R + 0.25)\omega_p^2 - \omega_p\,(2.5\omega_R - 950) - 200\,\omega_R + 9.5\cdot10^4, \tag{13}$$

where 0.77 was not yet taken into account the dimensional factor. Comparing this expression with the expression (9) derived from the mathematical model of this system and introducing M=0.4 kg, K=0, the identification of the parameters of the rotor can be completed:

$$\begin{aligned} m &= m(\omega_R) = (1.4\cdot10^{-3}\,\omega_R - 0.21) \text{ [kg]} \\ d_t &= d_t(\omega_R) = -(1.9\,\omega_R - 730) \text{ [kg/s]} \\ k_r &= k_r(\omega_R) = (7.3\cdot10^4 - 150\,\omega_R) \text{ [N/m]}. \end{aligned} \tag{14}$$

The Quadrature Impedances (Fig. 5) were identified as the straight lines; varying with rotational speed.

$$Q = (970 - 0.69\omega_R)(\omega_p - \lambda\omega_R), \tag{15}$$

where

$$\lambda = \frac{\omega_p\big|_{Q=0}}{\omega_R} \tag{16}$$

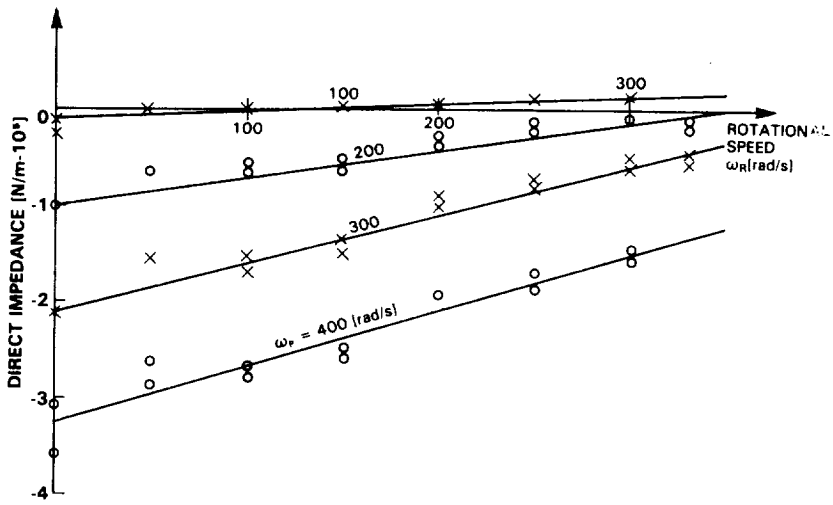

Figure 6. - Direct impedance versus rotational speed and variable perturbation speed.

is the ratio of the perturbation speed for which the Quadrature Impedance has a zero value to the rotational speed ω_R. The parameter λ appeared to be nearly constant for all performed tests: $\lambda = 0.48$.

Its value agrees with the oil whirl ratio observed in practice. The value $\lambda\omega_R$ corresponds to the average oil velocity.

The comparison between the expressions (10) and (15) leads to the identification of the system parameters:

$$d_r = d_r(\omega_R) = (970-0.69\ \omega_R)\ [kg/s]$$

$$k_t = k_t(\omega_R) = (470 - 0.33\ \omega_R)\ [kg/s] = \lambda d_r(\omega_R) \qquad (17)$$

and $m_t = 0$, as it has been already assumed.

As we notice, all parameters of the system are functions of the rotational speed ω_R. It was not possible to obtain test results for very low values of the perturbation speed. For this reason a "displacement" test was performed. The main shaft rotating at constant speed was perturbed by a constant pulling force P. The probes measured vertical and horizontal displacements. The force-response characteristics showed to be linear in relatively wide range of displacements, however, their slopes varied considerably with the rotational speed. The formula (11) served for the identification the parameters k_r and k_t (K=0 in this test*):

$$\begin{aligned} k_r &= 4000\ N/m\ (\text{for } 0 < \omega_R \leqq 150\ rad/s) \\ k_t &= (\ 490-0.27\omega_R)\ [kg/s]. \end{aligned} \qquad (18)$$

The evaluation of the coefficient k_r was not very precise. However, its relatively

* The calculation of the coefficients k_r and k_t was performed indirectly. First the slopes of the straight lines corresponding to the pulling force P_1 versus horizontal (x) and vertical (y) displacements were evaluated for different values of the rotational speed.
The slopes are equal to "directional" stiffnesses $K_x = P_1/x$, $K_y = P_1/y$, corresponding to x and y. Taking (6) and (11) into account the stiffness coefficients

$$k_r = K_y / (1+(K_y/K_x)^2), \qquad k_t\omega_R = k_r K_y/K_x$$

were then calculated for each value of the rotational speed.

small value was noticed especially for higher ω_R . The agreement with the previously evaluated coefficient k_t (expression (17)) is very good.

Having evaluated the parameters of the system the stability check has been possible.

Introducing the expressions (14) and (17) into the stability criterion (5) and rearranging terms, we obtain the cubic polynomical inequality:

$$1.29\ \omega_R^3 + 3030\ \omega_R^2 - 6.17 \cdot 10^5 \omega_R - 2.29 \cdot 10^8 < 0 \qquad (19)$$

The polynominal (19) has one positive root ω_R = 366 rad/s. The stability criterion, then, has the form: $\omega_R < 366$ rad/s.

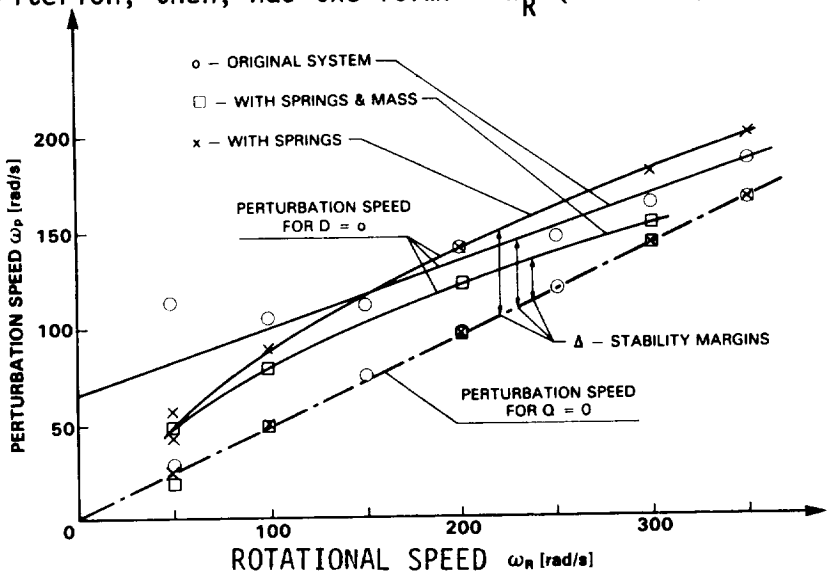

Figure 7. - Perturbation speed at zero impedances and stability margins.

During the experiment it was observed that for rotational speeds higher than 350 rad/s the rotor became unstable, which is consistant with the above analysis.

We notice that the value of amplitude peaks is closely related to the difference between perturbation speeds at which Direct Impedance and Quadrature Impedance equal to zero (Figs. 3 and 4). This difference is referred to as the stability safety margin Δ (see Appendix). In Fig. 7 the values of perturbation speed for zero impedances have been plotted. The margin of stability decreases with the rotational speed. For the considered systems ("0","S", and "SM") the zeros of the Quadrature Impedance remain the same. The additional springs and mass have influence on the Direct Impedance only.

At the reverse perturbation speed, the Quadrature Impedance is negative for all speeds (compare (10) for ω_p negative, see also Figs. 4 and 5). It does not cross zero; the system is very stable.

Figure 8 presents the impedances for the squeeze film test (ω_R=0). We notice the symmetric parabolic shape of the Direct Impedance and antisymmetric (straight line) for the Quadrature Impedance. (Slight displacement of the lines from zero at ω_p =0 is due to very low input force level). As expected, tangential stiffness, being related to the rotational speed, equals zero when ω_R=0.

In the squeeze film test the Quadrature Impedance contain then only the radial damping term d_r (see (10)), which appears to be positive. The condition of stability (5) is satisfied for all rotational speeds. The displacement of the

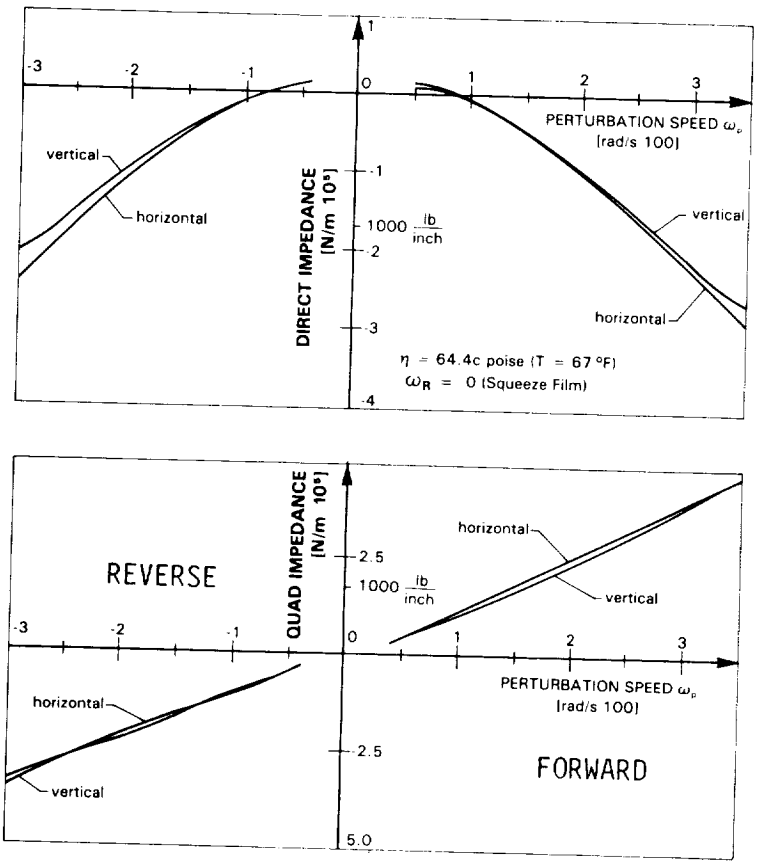

Figure 8. - Impedances versus rotational speed for squeeze film.

Direct Impedance parabole from the symmetric position for $\omega_R=0$ into the region of positive perturbation speeds for $\omega_R>0$ indicates a relationship of the tangential damping d_t with rotational speed. $d_t=0$ for $\omega_R=0$ and $d_t>0$ for $\omega_R>0$ within the investigated range of speed. (See (14) for comparison).

The Fig. 9 presents the Direct and Quadrature Impedances for variable oil temperature. The variations of the Quadrature Impedance are quite significant while the Direct Impedance remains nearly invariable in the wide temperature range, especially for lower values of the perturbation speed. Let us evaluate the Quadrature Impedance as a function of temperature. From the graphs Fig. 9 the relation between the slope of the Quadrature Impedance versus temperature and the speed ratio λ can be obtained. Finally the Quadrature Impedance is evaluated as follows [15]:

$$Q/0.77 = (1700 - 10T)\ [\omega_p - \lambda(T)\omega_R]\ [N/m],$$

$$\lambda(T) = 0.48\ (1.1 - 1.8\cdot 10^{-3} T),$$

where T is temperature in Farenheit degrees. Further we derive the relationship between temperature and oil viscosity (measured by Cannon-Fenske Viscosimeter 200), so that the Quadrature Impedance can be expressed in terms of the oil viscosity. If the Direct Impedance is known for any temperature, then a correcting factor can be introduced for the value of Direct Impedance corresponding to any different temperature [15].

Summarizing the test results, we see that the predicted model well reflects the main dynamic features of the system. The Direct and Quadrature Impedances can be identified easily as a function of the system parameters and in particular, as a function of the rotational speed.

ACTIVE SERVOMECHANISM CONCEPT

The ability of a lubricated bearing to support both steady-state and dynamic loads by forming a springy cushion consisting of a fluid wedge is well known. It is also well known that a 360° lubricated bearing has a propensity for instability known as oil whirl/whip. In fact, even before the outstanding work of Newkirk and Taylor [10] or Hull [11-13], Harrison [14] predicted in 1919 that the full lubricated bearing would be unstable.

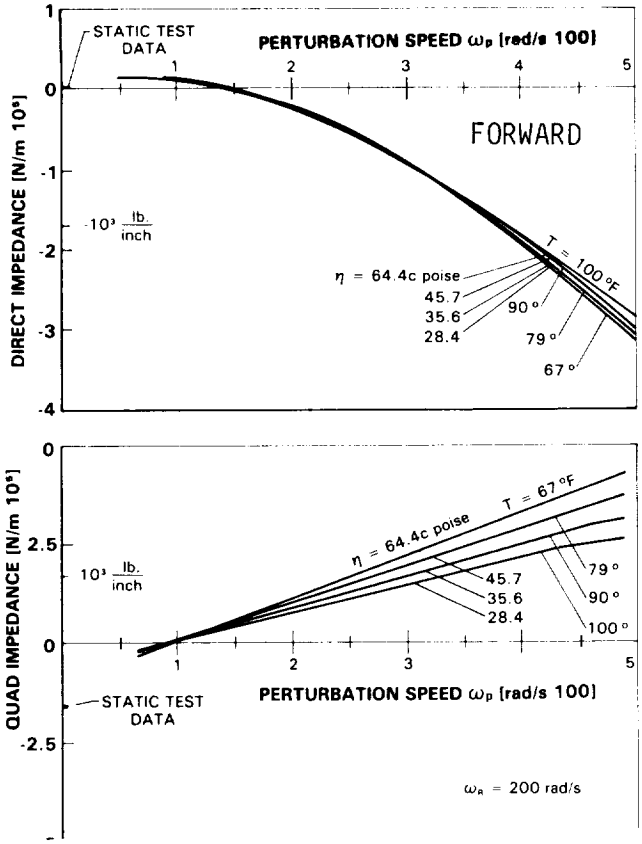

Figure 9. - Impedances versus perturbation speed with variable viscosity (temperature) of the oil.

The study of rotor instability has generated a vocabulary including such expressions as cross springs, cross damper, (and even cross masses), negative damping, etc. Such cross actions exist as effects, unlike gyroscopic action which is a genuine cross coupling physical law. The reason why these cross coupling bearing and seal effects occur is that such elements clearly have a behavior much more complex than any possible passive systems. These machine elements contain active feedback, in which exists a mechanism transferring rotational energy into lateral vibration energy. This is true for every identifiable rotor instability of the forward circular whirl and whip category, including shaft internal friction, aerodynamic cross coupling or steam whip. In particular, the behavior of a 360° lubricated bearing is analyzed herein. The situation in any gas or liquid seal is also generally in the 360 degree category so that the results can then be extended to any seal or bearing dynamic behavior. To show in simple description that such systems are actually closed loop servomechanisms, observe the performance of the bearing in response to a steady-state load.

Apply a downward pressure to a shaft rotating anticlockwise with no initial dynamic or steady-state preload. The obvious and well known result is that the shaft moves downward very slightly, and moves strongly to the right. This motion, of course, provides the converging lubricant wedge to support the applied downward load. Since lubricant has virtually no spring effect of its own, the action generates the spring cushion synthetically. Applying a downward steady-state load as a step function, the first effect is for the shaft to move downward in response to passive direct (radial) damping (d_r) . The result of this downward action is to create a restriction of oil flow at the bottom. This in turn creates a converging wedge on the left, which forces the shaft to the right. This process continues (usually with some damped whirling), until the shaft reaches an equilibrium position in which forces are balanced. This position to the right is sufficient to create the constriction which provides the wedge to support the shaft against the input force because the input to the active element is motion and the output is force, as previously described.

The dimensions of the active elements are that of impedance. It then seems reasonable to present the rotor/bearing system as a servomechanism with a feedback loop containing active elements of the system (Fig. 10). The general transfer

function of the system (described by Eqs. (1) and (4)) is given in the Appendix. As it has been shown in the previous section, the parameters related to the bearing depend directly on rotational speed - they represent active elements. The term "active" refers to the mechanism of transformation of rotational energy into vibration energy, which provides the major reaction to input forces.

The input to the system is represented by the exciting periodic force as well as static load ($\phi(\omega_p i)$ - see Appendix).

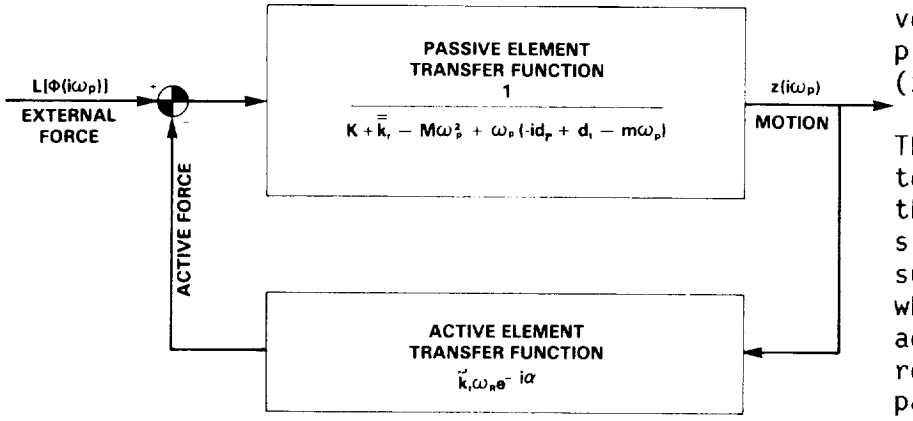

Figure 10. - Rotor-bearing active feedback diagram.

The output is the motion - vertical and horizontal displacements of the main shaft ($z(i\omega_p)$).

The output motion with respect to the input force shows all of the active and passive terms in simple series (see (A8)). As such, it could be optional which ones are put in the active category, with the remaining ones left in the passive category. However, the static loading test provides a perturbation speed of $\omega_p=0$ so that all terms containing ω_p as a multiplier are deleted. These terms deleted entirely are the passive terms. Further, the squeeze film tests, where rotative speed $\omega_R=0$ deletes all terms containing ω_R as a multiplier. The terms which are deleted entirely can be considered as the active terms. These observations indicate the proper location of the terms.

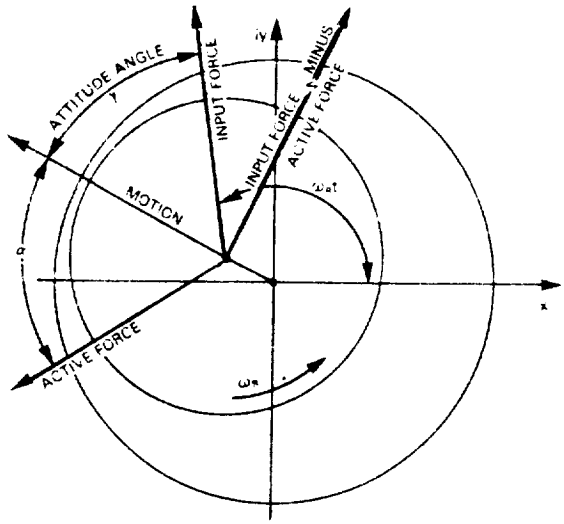

Figure 11. - Force diagram for rotational speed below resonance.

If a further check is desired, since it is fundamental that springs with negative stiffness cannot exist as real passive impedances, any negative stiffness term component necessarily represents the active portion of the feedback loop. Since spring force is motion times spring coefficient, in order to supply the restoring force against input force the elastic force must be at nearly 90 degrees with respect to motion, because the motion itself is nearly 90 degrees with respect to input force (Fig. 11).

As a result, the so called "cross spring" is actually the very real (but synthetically manufactured by feedback) restoring spring force. In review of the active behavior of such a bearing it is at the same time extremely simple with only one moving part, as well as extremely complex, because this one working part performs several functions.

Summarizing these considerations we describe the transfer function of the active feedback loop in the following form (Fig. 10):

$$\bar{k}_r - i\omega_R \tilde{k}_t \sin\alpha = \tilde{k}_t \omega_R (\cos\alpha - i \sin\alpha) = \tilde{k}_t \omega_R e^{-i\alpha}, \tag{20}$$

where $\bar{k}_r = \tilde{k}_t \cos\alpha$, $k_r = \bar{k}_r + \bar{\bar{k}}_r$, $k_t = \tilde{k}_t \sin\alpha = \lambda d_r$.

The active loop then contains a fraction of the ω_R dependent coefficient k_r (radial stiffness) and full tangential stiffness coefficient. The last one is entirely the result of oil wedge formation. As it was identified in the previous section, the radial stiffness contains a constant term and a term varying with the rotational speed. However, a precise identification was difficult in view of its relatively small value.

It is supposed that the terms located in the feedback loop are directly responsible for the transfer of rotational energy into vibrations. The angle α represents the angle between the observed motion and the active force (Fig. 11). This angle is usually a little less than 90 degrees for 360° fluid bearing. For other types of bearings it is nearer 0 degrees (e.g. for sleeve bearings with stable void islands in the thick film region, generally referenced to as "180 Degree" or "Half Sommerfeld" bearings).

In the present study it has been found that the radial spring coefficient has a low value, for $\alpha \cong 90°$ $\cos\alpha$ is very small - this is reflected in the expression (20). However, at this time we have not found a means to measure directly the angle α.

All other terms of the rotor system are located in the "passive" part of the servomechanism model (Fig. 10). Being functions of the rotational speed, they may also modify the rotor response in some "active" way, however to a lower degree than the ones related to stiffnesses.

A rotating shaft in a bearing does (1) have passive impedance, (2) transfers energy from input torque by dragging lubricant around, (3) moves sidewise of the input force (as best it can) to provide a restriction of flow to the lubricant to build a converging wedge for support, and finally (4) synthetically builds a force to counteract the input force.

Rotor systems, as currently configured, are rarely well stabilized because (1) their basic algorithims are complex, nonlinear and nonsymmetric, and (2) there has been lack of recognition and knowledge of this feedback nature of rotor behavior. The present paper throws some light on these problems, however much more research is needed to provide answers to all questions related to the rotor/bearing/seal stability.

REFERENCES

1. Tondl A., "Some Problems of Rotor Dynamics", Czechoslovak Academy of Sciences, Prague 1965.
2. Vibrations in Rotating Machinery, Proc. of the Conference, University of Cambridge, The Institution of Mechanical Engineers, Cambridge, U.K., 1976.
3. Rieger, N.F., "Rotor-Bearing Dynamics: State of the Art 1976", Shock and Vibration Digest, v. 9, No. 5, 1977.
4. "Rotordynamic Instability Problems in High Performance Turbomachinery", Proc. of a Workshop, Texas A & M University, College Station, Texas, 1980.
5. Tribology International, 0301-979X/80/050233, JPC Business Press, October 1980.

6. Hankey, W.L., "Self Excited Oscillation in Fluid Flow", University of Dayton Research Institute Seminar, May 1981.
7. Bently, D.E., Bosmans, R.F., "Oil Whirl Resonance", Trans ASME, April 1979.
8. Bently, D.E., "The Parameters and Measurement of the Destabilizing Actions of rotating Machines and the Assumptions of the 1950's", in [4].
9. Kanaki, H., Mitsubishi Heavy Industries, LTD, Takasayo, Private communication, 1981.
10. Newkirk, B.L., Taylor, H.D., "Shaft Whipping Due to Oil Action in Journal Bearings", G.I. Review, v. 28, 1925.
11. Hull, E.H., "Oil Whip Resonance", Trans ASME, October 1958, pp. 1490-1496.
12. Hull, E.H., "Journal Bearing Behavior Under Periodic Loading", G.I. Research Laboratory, Rep. No. 55-RL-1354, Schenectady, New York, 1955.
13. Hull, E.H., Darrow K.A., "Hydrodynamic Oil Film Stiffness", G.I. Research Laboratory, Rep. No. 59-RL_2217, Schenectady, New York, 1959.
14. Harrison, W. J., "The Hydrodynamic Theory of the Lubrication of a Cylindrical Bearing Under Variable Load", Trans Cambridge Philos. Soc., v. 22, 1919.
15. Bently, D.E., Muszynska, A., "Stability Analysis of Cylindrical 360° Bearing Oil Whirl", Bently Nevada Report, 1982 (to appear).
16. Adams, M.L., Padovan J., "Insights Into Linearized Rotor Dynamics", Journal of Sound and Vibration, 76 (1), 1981.
17. Lund, J.W., Thomsen, K.K., "A calculation Method and Data for the Dynamic Coefficients of Oil Lubricated Journal Bearings", Topics in Fluid Film Bearing and Rotor Bearing System Design and Optimization, ASME, 1978.
18. Childs, D.W., Dressman, J.B., "Testing of Turbulent Seals for Rotor Dynamic Coefficients," in [4].

APPENDIX

AI. EIGENVALUE PROBLEM FOR THE EQUATIONS (1) AND (4)

The homogeneous equation (1) with hydrodynamic forces (4) has the following eigenvalues:

$$\lambda_{1,2,3,4} = (-d_r \pm i(d_t - J_1\omega_R - J_2\omega_p))/(2M+2m) \pm (\alpha_1 + i\alpha_2), \tag{A1}$$

where

$$\alpha_j = \Big[(-1)^j \left((d_t - J_1\omega_R - J_2\omega_p)^2 - d_r^2 + 4((M+m)k_r + m_t k_t \omega_R)\right) + \\ + \left(((d_t - J_1\omega_R - J_2\omega_p)^2 - d_r^2 + 4((M+m)k_r + m_t k_t\omega_R))^2 + \right. \\ \left. + 4\left(d_r(d_t - J_1\omega_R - J_2\omega_p) + 2(m_t k_r - (M+m)k_t\omega_R)\right)^2\right)^{\frac{1}{2}} \Big]^{\frac{1}{2}} / (\sqrt{8}(M+m)), \quad j=1,2. \tag{A2}$$

The condition of stability (negative real parts of the equinvalues (A1) is as follows:

$$d_r((M+m)k_r + m_t k_t\omega_R) - d_r(d_t - J_1\omega_R - J_2\omega_p)(m_t k_r - (M+m)k_t\omega_R) - (m_t k_r - (M+m)k_t\omega_R)^2 > 0. \tag{A3}$$

For $J_1 = J_2 = m_t = 0$ it reduces to

$$-(M+m)(k_t\omega_R/d_r)^2 + k_t\omega_R d_t/d_r + k_r > 0\,, \tag{A4}$$

or after transformation to

$$-|f_2| < \omega_R k_t/d_r < |f_1|\,, \tag{A5}$$

where

$$f_j = \pm\left[\, d_t/(2M+2m) + (-1)^j\left((d_t/(2M+2m))^2 + k_r/(M+m)\right)^{\frac{1}{2}}\right], \quad j=1,2 \tag{A6}$$

are natural frequencies of the system at the limit of stability, i.e., when instead of inequality (A4) we have the equation. As we can easily check f_1 and f_2 are also the roots of the Direct Impedance (9).

For $k_t > 0$ the quantity

$$\Delta = f_1 - \omega_R k_t/d_r > 0 \tag{A7}$$

gives a margin of safety for the stability. As the value $\omega_R k_t/d_r$ is the root of the Quadrature Impedance (10), the stability of the perturbed system is assured if the zero of the Quadrature Impedance appears at a lower perturbation speed ω_p than the zero of the Direct Impedance.

AII. FOURIER TRANSFORMATION OF THE EQUATIONS (1) and (4).

The mathematical model of the system can be presented applying the Fourier transformation and the control theory formalism. From (1) and (4) we get then

$$z\,(i\omega_p)\;\;[D\,(i\omega_p) + iQ\,(i\omega_p)] \quad = L\;\;[\,\emptyset\,(i\omega_p)] \tag{A8}$$

where $z\,(i\omega_p)$ is the Fourier transformation of the variable z(t) (2), $i\omega_p$ is the Fourier operator, $D(i\omega_p)$, $Q(i\omega_p)$ are given by (9),(10), $L\,[\,\emptyset\,(i\omega_p)]$ is the Fourier transformation of the input forces $\emptyset = U\omega_p^2\, e^{\,i\omega_p t} - iP_1$. $[D(i\omega_p) + +iQ\,(i\omega_p)]$ is the transfer function of the system.

NOTATION

A	Amplitude of the response
C	Bearing radial clearance (0.015"=3.8 10^{-4} m)
d_r, d_t	Radial and tangential bearing damping coefficients
D	Direct Impedance
g	Acceleration of gravity
I_1, I_2	Moments of inertia of the main (1) and perturbing (2) shafts about x or y axis (24.8 gm^2, 6.7gm^2; I_1=50 gm^2 for the case of additional mass)

I_{1z}, I_{2z}	Moments of inertia of the main and perturbing (2) shafts about the axis of rotation ($0.0650 gm^2, 0.03 gm^2$; $I_{1z}=0.0652 gm^2$ for case of additional mass)
k_r, k_t	Radial and tangential bearing stiffness coefficients
K	Equivalent stiffness coefficient of the additional springs (33100 N/m=189 lb/inch)
l_1	Length of the perturbing shaft (9.5"=0.241m)
l_2	Distance from the center of bearing to the probe (0.625"=0.0159m)
l_3	Distance from the bearing center to the pulling force section (2"=0.0508m)
l_4	Length of the main shaft (11.75"=0.298m)
l_5	Distance to the position of the perturbing force (7.7"=0.195m)
m_1, m_2	Masses of the main and perturbing shafts with accessories (280g, 150g)
m_p	Perturbing unbalance mass (4g)
m_r, m_t	Radial and tangential bearing "fluid inertia" coefficients
"0"	Original system
P	Pulling force
Q	Quadrature Impedance
r	Radius of the controlled unbalance (33/32"=0.0262m)
R	Radius of the shaft journal (1.00"=0.0254m)
"S"	System with additional springs
"SM"	System with additional springs and mass
γ	Phase of the response - Attitude angle
Δ	Stability margin
η	Dynamic viscosity of oil (poise)
λ	Oil rotation speed ratio
ω_p	Perturbation speed (perturbing shaft)
ω_R	Rotation speed (main shaft)